24th COBEM - 2017

24th ABCM International Congress of Mechanical Engineering
December 3-8, 2017, Curitiba, PR, Brazil

COBEM-2017-2235
NUMERICAL ANALYSIS OF THE INFLUENCE OF OUTPUT ANGLES OF ROTOR BLADES ON CHARACTERISTICS CURVES OF A RADIAL PUMP

Luan de Lima Freire
Luís Morão Cabral Ferro
Universidade Federal Rural do Semi-árido, 572 Ave. Francisco Mota Mossoró, Rio Grande do Norte, 59625-900
luanfmp@hotmail.com
lferro@ufersa.edu.br

Abstract. *The use of computational tools for the solution of engineering problems has been growing in last years. Many of these problems deal with fluid flow, often incompressible, and a description of a complex geometry is need. In industry pumps are applied to increase the pressure of the fluids or to extract fluids from reservoirs, as in the oil industry, for example. Numerical methods can be used to evaluate the performance of pumps at different situations. . In this paper a Computational Fluid Dynamics (CFD) software available in ANSYS® is used to compute the flow through a rotor of radial pump of an oil with a dynamic viscosity of 582.75 cP and an absolute density of 925 kg/m3. Characteristics curves of total height, efficiency and brake horsepower as a function of volumetric flow rate for different output angles of the blades of the pump are computed and compared for three different angles of the blades. The domain of the fluid is discretized by a structured mesh. A mass outflow condition is prescribed at outlet section and the velocity direction is known at inlet section. No slip condition is used at the hub and the shroud surfaces and the periodic condition is used at the remaining surfaces. The turbulence is modulated by k-ε model. The computed characteristic curves for the three outlet angles are shown and are compared. Results for the velocity fields and meridional average total pressure are also shown and compared for the three outlet angles. The results show that the CFD was able to predict correctly the characteristic curves and can be used as a tool on the design of centrifugal rotor pumps.*

Keywords: *Aerodynamics, Computational Fluid Dynamics (CFD), Characteristic curves, Navier-Stokes equations.*

1. INTRODUCTION

Typically, the performance characteristics of centrifugal pumps are shown by curves, known as operating characteristics curves, and are provided by the manufacturers of pumps. Such curves usually are obtained by testing laboratories and available in technical catalogs (Monachesi, 2005). The experimental evaluation of characteristic curves of centrifugal pumps is expensive and a model of the rotor must be manufactured. An experimental facility and time consuming tests must be evaluated to get the referred curves. The *CFD* can be used to study the effect of any parameter on the performance of a pump. For example a numerical analysis of the influence of Reynolds number on the flow through the centrifugal rotor pump and the characteristic curves is presented by Bezerra and Ferro (2016).

The main characteristic variables, as total head *H*, input power *P* and efficiency η are function of the flow rate and of the geometry of the pump. The geometry of the pump is defined by the width of the rotor at inlet and outlet sections, by the blade angles as well as radial variation of these parameters. The thickness of the blades, the number of blades and the Reynolds number, viscosity of the fluid or rotational speed of the rotor, also have influence on the performance of a pump. Through the one-dimensional theory, it is possible to get results in studies of centrifugal pumps for operating points close to nominal condition using Euler theory and equations as well as empirical correlations. The development of *CFD* codes, the computing capacity growth combined with the creation of new software allows the easily and fast computation of three-dimensional viscous flows through the rotor of a centrifugal pump (Macintyre, 1997) and (Silva, 2000).

This paper proposes the numerical analysis of the influence of the variation of the output angle of the rotor blade of a centrifugal pump on the operating characteristic curves. The ANSYS® CFX (2013a) software is used to generate a computational mesh of a centrifugal rotor pump and to compute the flow of an oil with a dynamic viscosity of 582.75 cP and an absolute density of ρ=925 kg/m^3 Three rotors with different output angles β_2' are analysed. Characteristic curves are computed and compared.

2. METHODOLOGY

The main objective of the computational procedure was to obtain the characteristic curves of the rotor a centrifugal pump with three different angles of blades at the outlet section and to analyse numerically the influence of these angles on the shape of the characteristic curves. Three different curves, for each angle, have been computed: total head H versus volumetric flow rate Q, efficiency η versus Q and input power P versus Q. The values of outlet angles were chosen according with outlet angles on commercial rotor (Macintyre, 1997). Figure 1 shows the geometry of the rotors for the three different output angles and Fig 2 show the mesh for the rotor with an output angle β_2' =30º.

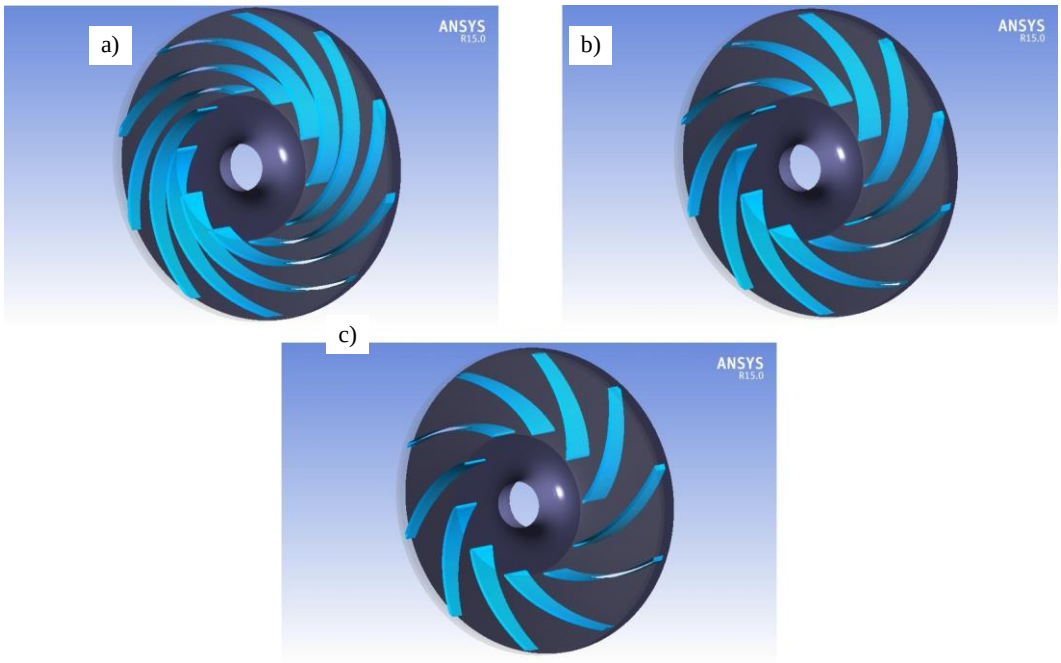

Figure 1. Geometry meshes with output angles of the blades: a) 20°, b) 30°and c) 40°.

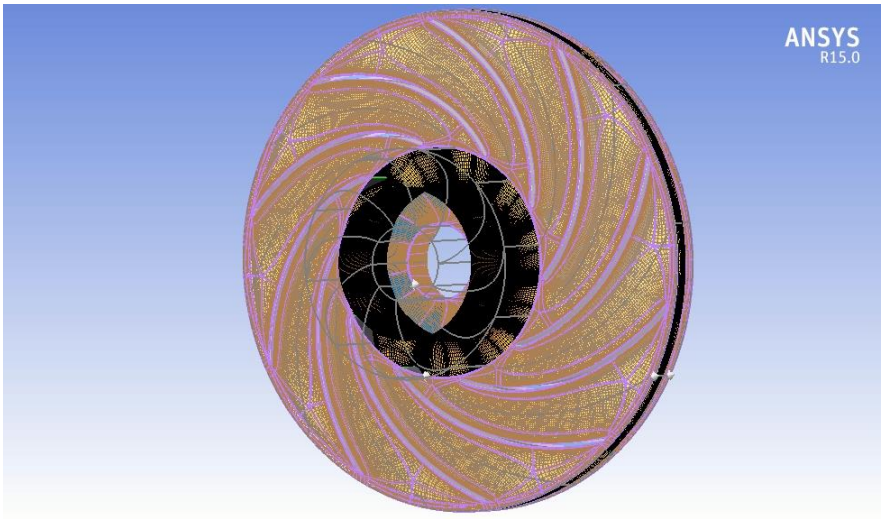

Figure 2. Geometry meshes of the rotor with β_2' =30

Table 1 shows the geometric characteristics of the rotors of three centrifugal pumps used in the simulations. The geometry was created through the *BladeGen* module. The dimensions of the rotor were defined using a meridional plane. In this module, the inlet and outlet fluid sections, the number of blades of the rotor and their thickness were also specified.

Table 1. Geometric characteristics of the rotors.

Description	Value
Rotor diameter at inlet section d_1	165 mm
Rotor diameter at outlet section d_2	345 mm
Shaft diameter d_n	54 mm
Blade inlet angle of the rotor β_1'	18.63º
Blade outlet angle of the rotor β_2'	20º / 30º / 40º
Number of blades Z	10
Blade constant thickness	4 mm
Width of the blade at inlet section b_1	49 mm
Width of the blade at outlet section b_2	22 mm

For each of the rotors shown at Fig. 1 a computational mesh was generated using *TurboGrid* (2013b) package. This package takes advantage of the sizing done in *BladeGen* and automatically generates a structured mesh suitable for the geometry. Structured meshes have a generation rule, requiring less computational effort to be developed, but the possibility of achieving a higher concentration of elements in a specific area is based on the use of unstructured meshes. The mean characteristics of the used meshes are presented in Table 2.

Table 2. Characteristics of computational meshes.

Output angle of the rotor	Number of nodes	Number of elements
$\beta_2' = 20°$	262320	238757
$\beta_2' = 30°$	313600	289850
$\beta_2' = 40°$	362950	338217

The fluid domain was discretized by a structured mesh with hexahedral elements. The solid boundaries of the fluid domain are the blades, the hub and the shroud of the pump. A detail of the computational mesh is shown in Fig. 3.

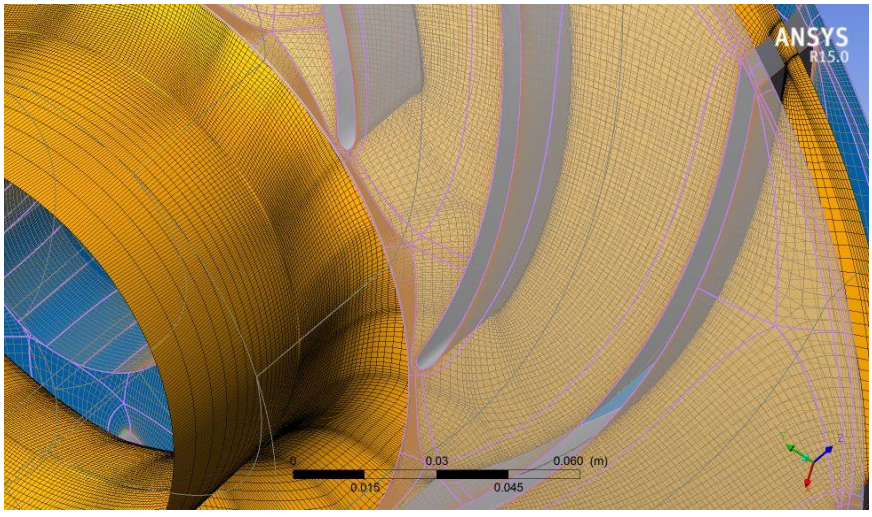

Figure 3. Detail of the mesh generated by *TurboGrid*.

The simulation of the flow through the pump was done in the CFX package that works with the most diverse types of simulations, in permanent and transient regimes, with and without heat transfer (ANSYS, 2013a). The machine used was an ASUS notebook with Intel® Core™ i3-2330M CPU @ 2.20 GHz processor, 4.00 Gb RAM and a 64-bit operating system.

For the computer simulation an oil was used as the working fluid. The properties of the fluid were taken from Santana *et al*. (2004). The density of the oil is ρ=925 Kg/m^3 and the dynamic viscosity μ=582.75 cP. The temperature of the oil is 268.15 K. The angular velocity of the rotor is 1450 rpm, for all the simulations, which is readily found in commercial pumps. The flow is assumed as steady and the turbulence modulated using standard *k-ε* model as the turbulence model (Launder and Spalding, 1974).

2.1 Boundary conditions

The boundary conditions define the behavior of the fluid in contact with the domain boundaries. For inlet condition, a total pressure of one atmosphere (1 atm) is prescribed for all simulations (*pressure inlet condition*). The boundary condition for the outlet section was defined based on its mass flow (*mass flow outlet condition*) and direction of the velocity normal to the boundary. Table 3 presents the values of the volumetric and mass flow rate used.

Table 3. Values of the volumetric (m^3/s) and mass flow rate (kg/s) used for numerical calculations.

$\dot{m}$ (kg/s)	13.87	27.75	34.69	41.62	48.56	55.50	69.37	83.25	97.12	111.00	124.87	138.75
Q (m^3/s)	0.015	0.030	0.0375	0.0450	0.0525	0.0600	0.0750	0.0900	0.1050	0.1200	0.1350	0.1500

The rotor blades, hub and shroud, for the purpose of this simulation, assumed the wall condition and obey the no-slip wall condition in which the relative velocity between the fluid and the boundaries is always zero. The fluid inlet channel assumed a wall boundary condition too. After the inlet section and before the rotor a cylindrical surface, coaxial with turbine is generated. A free slip wall condition is considered at this surface, allowing the fluid to enter the domain without the influence of rotation on it. This part of the geometry was inserted in the fluid domain to decrease the possible downstream influence of the rotor at the inlet section of the domain. Figure 4 shows the control volume and main defined boundaries on the control volume. In the lateral surfaces of the control volume periodic interfaces were considered.

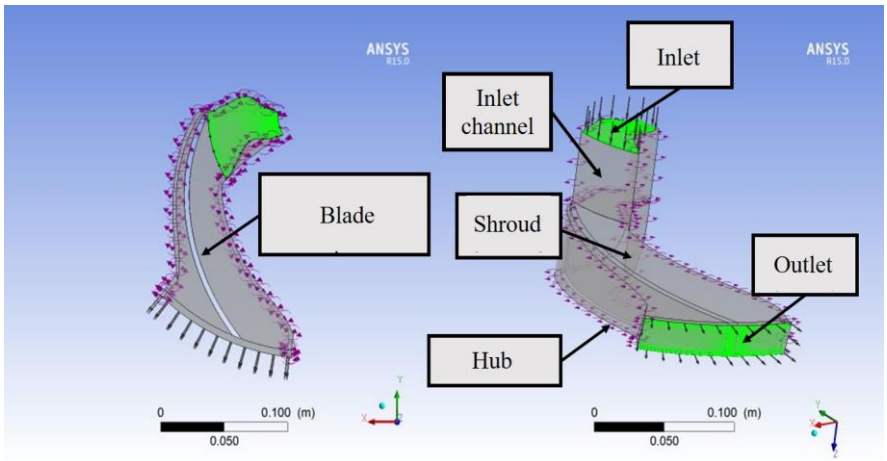

Figure 4. Boundaries defined in CFX.

In order to evaluate the residuals generated in the calculation of the conservation equations in the solver, RMS (Root Mean Square) was used as a convergence criterion, which is nothing more than the square root of the mean squares of residual values on the solution of continuity and momentum equations. The maximum value prescribed for the residuals in the simulations was 0.00005 with the minimum number of iterations of 1 and the maximum of 1000. To obtain better results, a double precision condition was applied to the solution.

In order to achieve better results, tests were carried out with several types of geometry and refinement of the computational mesh. Concerning the position of the inlet section of the rotor, the geometry did not initially have cylindrical channel and the results presented a recirculation effect during the solver application, which required even more computational work to be solved. Therefore, even if the final results were not significantly affected, insertion of

the inlet channel provided a major improvement. Figure 5 shows the meridional projection of the geometry with and without inlet channel.

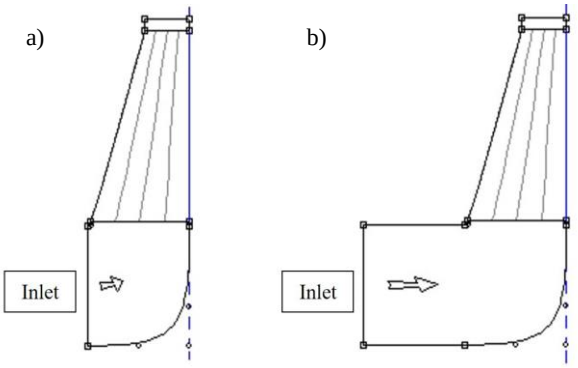

Figure 5. Meridional projection of the centrifugal pump: (a) without fluid inlet channel; and with fluid inlet channel.

The same kind of test was applied relative to the position of outlet section of the domain. A fluid outlet channel was generated (Fig. 6), but the effect of the recirculation on the exit, mainly for the lower values of flow rate, remained, not validating its use in the final geometry.

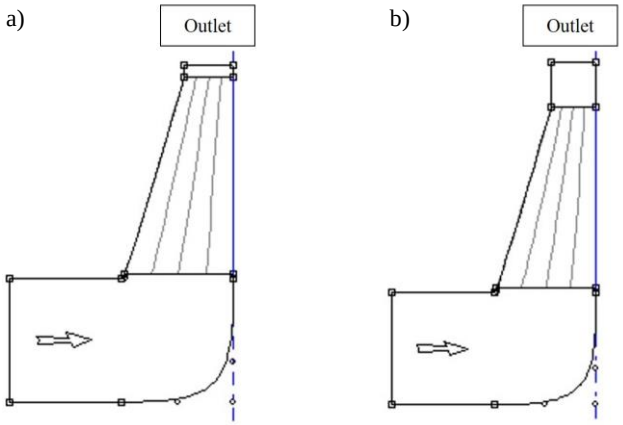

Figure 6. Meridional projection of the centrifugal pump: (a) without fluid outlet channel and (b) with fluid outlet channel.

The tests related to the refinement of the computational mesh showed that the CPU time of the simulations increased quickly with the increase of the number of elements in the mesh. The choice of refinement was motivated by the possibility of application in machines with lower computational capacity and also by the number of tests that were performed to obtain the characteristic curves.

3. RESULTS

The results of the simulations were obtained using the CFX package. It was possible to obtain the representation of streamlines, pressure and velocity fields, as well as tables and graphs with flow parameters. All simulations converged before the stipulated maximum number of iterations has been achieved (1000 iterations).

The values of both processing time (*CPU*) and total number of iterations grow when the output angle of the rotor β_2' increase. This phenomenon is due the increase of the total number of elements that occurs as the exit angle increases, causing a direct effect on the processing time.

The graphs of total head H versus volumetric flow rate Q are presented in Fig. 7 for the three angles β_2'. It was possible to notice that the total head increases with the increase of β_2'. This phenomenon is due the increase of energy supply to the fluid by the rotor with the increase of this angle. The difference between the total H of the three geometries, at a specified flow rate, increases with the flow rate due the increase of losses and the decrease of efficiency.

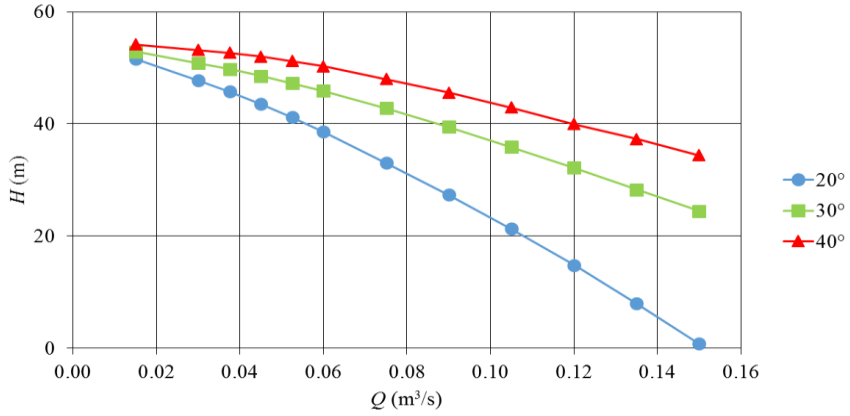

Figure 7.Computed characteristic curves of total height *H* versus volumetric flow rate *Q* for the three rotors.

The results for the characteristic curves of the input power supplied by the rotor *P* versus the volumetric flow rate *Q* are plotted in Fig. 8. Figure 8 shows that with the increase of the exit angle of the blades, higher power values are achieved.

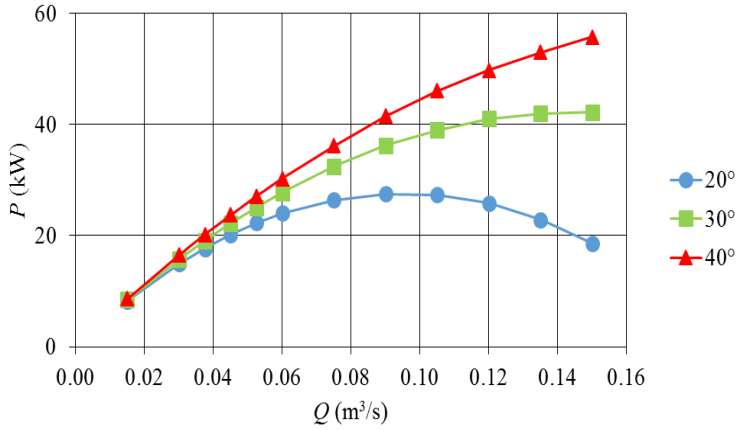

Figure 8. Computed characteristic curves of input power *P* versus volumetric flow rate *Q* for the three rotors

The characteristic curves for efficiency obtained through the simulations for the studied geometries are shown at Fig. 9.

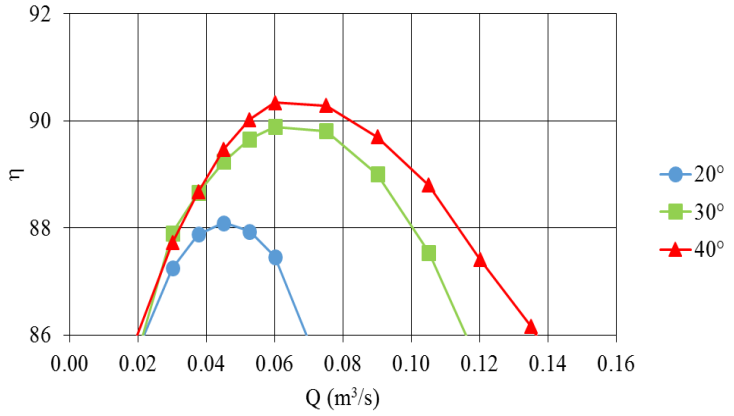

Figure 9. Computed characteristic curves of efficiency η versus volumetric flow rate *Q* for the three rotors.

As the pumps are designed to work at maximum efficiency, this characteristic is analysed in this work. Table 4 presents the nominal characteristics ($\eta=\eta_{max}$) for each computed geometry. The maximum efficiency increases when the

output blade angle increases. The operating range, i.e. the range of flow rates at which the pump can operate, becomes larger when the outlet β_2' increases, as presented at Figure 9.

Table 4. Nominal efficiency characteristics as function of output blade angles.

Output angle of the rotor β_2'	Nominal flow rate Q	Maximum efficiency η
20°	0.045 m^3/s	88.09%
30°	0.06 m^3/s	89.89%/
40°	0.06 m^3/s	90.33%

In addition to the analysis of the characteristic curves, the analysis of the velocity vectors field was also carried out under conditions of maximum efficiency. Figure 10 shows the velocity vectors of the three geometries for a mean span wise section of 50% of the span width of the rotor.

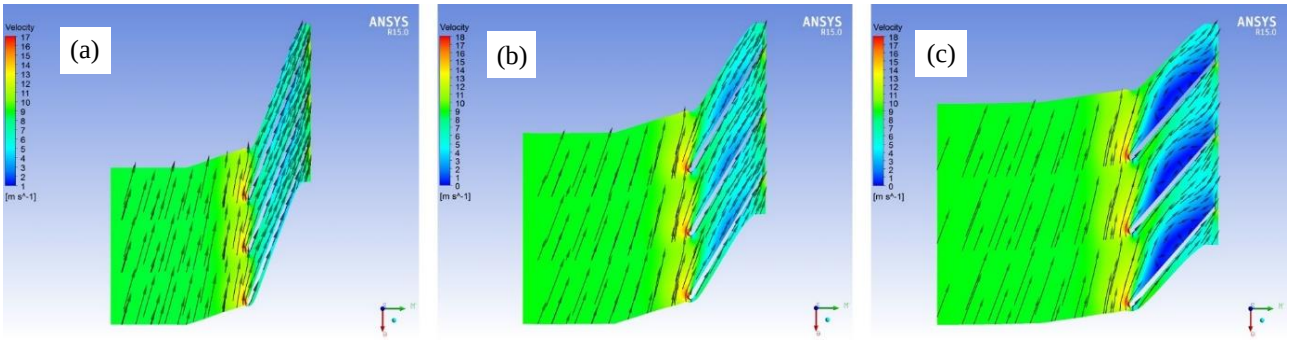

Figure 10. Velocity field diagrams at mean spanwise section of the rotor for: (a) β_2' =20º; (b) β_2' =30º and (c) β_2' =40º

Through the analysis of these representations, the reduction of kinetic energy, characteristic of centrifugal pumps, obtained by reducing the velocity in the areas near the rotor blades, was verified, proving that the model meets the slip wall condition on the walls of blades, imposed on pre-processing. This reduction can be visualized by the color scale in the upper left corner of the images, with the shades of blue representing the lower speeds, those of green the intermediate ones and those of red the relatively high speeds. The recirculation effect is most evident in the representation of the geometry with an exit angle of 40 °.

Figure 11 presents the total pressure isolines of average meridional flow for the three geometries of the rotor. In this figure the radial positive pressure gradient is clearly visible. The gradual increase of the pressure in the rotor can be visualized by the color representation of isolines. These graphs of Fig. 11 show that isobaric surfaces are almost cylindrical surfaces that are coaxial with the rotor axe. As expected the graphs shows that maximum pressure on the rotor, outlet pressure increases when the outlet angle β_2' increase. The results for the three rotors show that the pressure distribution and consequently the flow are almost independent of span wise coordinate.

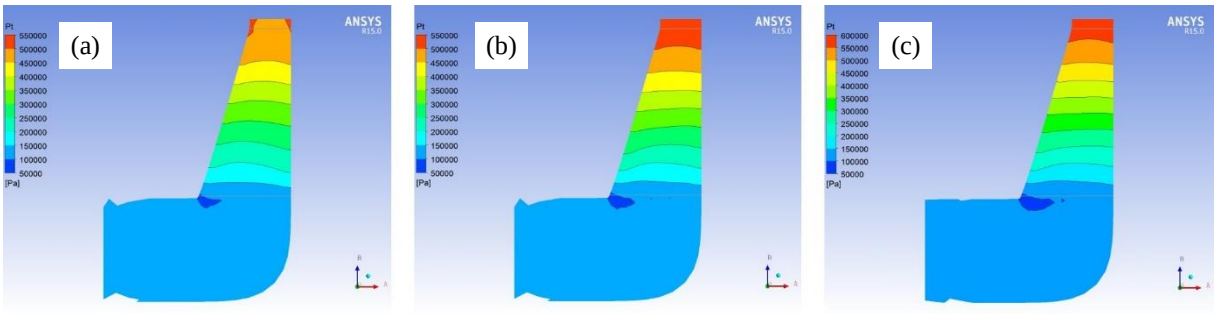

Figure 11. Isolines of total pressure on the meridional surface for (a) β_2' =20º; (b) β_2' =30º and (c) β_2' =40º

Table 5 presents the values of the dimensionless coefficients of flow rate φ, total head ψ and input power X for each output angle of the rotor β_2' analysed. Also the values of degree of reaction G and slip factor σ stipulated for maximum efficiency (η_{max}) are presented. The results agree with theoretical expectation with reduction of degree of reaction with increase of outlet angle of the rotor (0.669 for β_2' =20º to 0.621 for β_2' =40º).It is also possible to note that when the pump outlet angle increases, the slip factor increases too.

Table 5. Dimensionless coefficients at nominal conditions and degree of reaction G for the three rotors analysed

β_2'	φ	ψ	X	η_{max} (%)	G	σ
20º	0.0097	0.1383	0.0015	87.45	0.67	0.85
30º	0.0097	0.1643	0.0018	89.89	0.66	0.86
40º	0.0072	0.1863	0.0015	89.47	0.62	0.89

4. CONCLUSION

The flow through the three rotors of a centrifugal pump with outlet angles β_2' =20º, β_2' =30º and β_2' =40º is computed using ANSYS CFX code with k-ε model. Smooth characteristic curves of total head, input power and efficiency versus volumetric flow rate are obtained. An increase of the values of maximum efficiency with the output angle is verified. Velocity field diagrams at mean span wise section of the rotor for the three angles are computed and compared. Isolines of total pressure of the meridional flow are computed and shown. The results have good agreement with one-dimensional theory with a small variation of pressure and velocity on span wise direction. The computed values for the degree of reaction for each of the rotors are consistent with literature.

The Computational Fluid Dynamics and the ANSYS CFX code were used with success and consistent results on the computation of the characteristic curves of a centrifugal rotor and can be used in the improvement of the geometry of this type of pumps. Computational Fluid Dynamics can be used as an alternative of experimental tests on the design of the rotor of a centrifugal pump

5. ACKNOWLEDGMENTS

The authors would like to express their acknowledgements to Federal Rural University of Semi-Árido (UFERSA) and to Engineering Center of UFERSA for the financial support.

6. REFERENCES

ANSYS, 2013a. *ANSYS CFX User's Guide. Release 15.0*. ANSYS Inc. Southpointe.

ANSYS, 2013b. *ANSYS TurboSystem User's Guide. Release 15.0.* ANSYS Inc. Southpointe.

Bezerra, I.S. and Ferro, L.M.C., 2016. "Estudo numérico da influência do número de Reynolds nas curvas características de funcionamento em um rotor de uma bomba centrífuga". In *Proceedings of the IX Congresso Nacional de Engenharia Mecânica (CONEM)*. Fortaleza, Brazil.

Launder, B.E. and Spalding D.B., 1974. "The numerical computation of turbulent flows". C*omputer Methods in Applied Mechanics and Engineering*, Vol. 3, No. 2, p. 269–289.

Macintyre, A.J. , 1997. *Bombas e Instalações de Bombeamento*. LTC, Rio de Janeiro 2nd Edition.

Monachesi, M.A., 2005. *Eficiência Energética em Sistemas de Bombeamento*, Eletrobrás, Rio de Janeiro.

Santana, C.W.S., Torres, E.G. and Lacerda, I.S., 2005. "Ajuste de equações para a viscosidade cinemática de produtos de petróleo em função da temperatura". In *Proceedings of the Anais do 3° Congresso Brasileiro de P&D em Petróleo e Gás*. Salvador, Brazil.

Silva, J.B.S., 2000. *Pré-projeto de rotores de máquinas de fluxo geradoras radiais*. Graduation monograph, Mechanical Engineering, Paulista State University, Brazil.

7. RESPONSIBILITY NOTICE

The authors are the only responsible for the printed material included in this paper.